



POLITECNICO
MILANO 1863

**SCUOLA DI INGEGNERIA INDUSTRIALE
E DELL'INFORMAZIONE**



Python aided structural performance-based design optimisation of a secondary mirror for a Concentrated Solar Power (CSP) plant

**PYTHON DRIVING LICENSE
PROJECT**

Lucio Pinello

Professors:
G. Raos, E. Miglio, F. Bruschi

Academic year:
2022-2023

Abstract: Concentrated Solar Power (CSP) plants use mirrors to reflect and concentrate sunlight onto a receiver, to heat up a fluid and store thermal energy, at high temperature and energy density, in order to produce dispatchable heat and/or electricity. The secondary mirror is a critical component in the optical system of certain Solar Power Tower plants (SPT), as it redirects the concentrated sunlight from the primary mirror onto the receiver, which can be arranged at ground level. In this study, we propose a design optimization for the secondary mirror of a CSP plant. The design optimization method consists of two steps. The first step involves the use of finite element simulation software to analyze the structural performances of the secondary mirror under thermal loads and wind. The second step consists of using simulation results to identify the combination of design parameters and best performances, with respect to design constraints and structural safety. This is done by developing a Python algorithm that selects the configurations that satisfy the constraints.

1. Introduction

Concentrating Solar Power (CSP) systems represent one of the most promising technologies to take advantage of solar energy. Among them, Solar Power Tower (SPT) uses mirrors to concentrate direct sunlight in a focal point, obtaining intensive and highly variable direct solar power fluxes, that are transferred to a heat transfer fluid [1],[2]. Heat storage systems integrated into CSP plants allow for generating heat and/or electricity not only during sunny hours but on demand. To achieve the high temperatures required for steam generation, the solar radiation must be concentrated using effective methods, based on accurate design and fabrications. The technological challenge in the solar field is to ensure the required optical precision and simultaneous robustness against environmental influences, such as wind and temperature fluctuations, at the lowest possible cost [3]. Among the SPT configurations, the beam-down technology is currently attracting increasing interest worldwide: the sunrays reflected by the heliostats field point to a secondary mirror, that reconcentrates the solar radiation into the receiver, which is placed on the ground rather than on top of the tower. The beam-down technology allows to obtain of a greater concentration of sunlight and helps to reduce maintenance and operating costs, compared to solar applications where reacting solids are involved or heavy equipment must be placed on top of conventional towers [4]. Beam-down installations have been realized in Japan, Israel, United Arab Emirates, China and Italy [5].

1.1. Beam-down mirror design and optimization

The thermal and mechanical design [4] of secondary mirrors is a critical topic in the optical system of beam-down plants. The main challenges for such mirror design are its high operating temperature, along with the need for high shape accuracy and reflectivity. Mirror severe temperatures evolve mainly due to the amount of irradiance that is being absorbed by the mirror and, to a lesser extent, due to convective heat exchange with the environment. Exposure to high flux densities originating from the primary concentration field, part of which is absorbed by the mirror, heats up the secondary mirror with daily cycles. Hence, the mirrors are exposed to environmental conditions such as humidity and dust, high radiation fluxes, and elevated temperatures; therefore they are subjected to thermal stresses, deformations, and degradation throughout the time. For most solar reflectors, exposure during service to sunlight, particularly to ultraviolet wavelengths, high temperatures, and moisture can lead to a loss in reflectance that would lead to even higher absorbed flux [9], and thus to secondary mirror overheating. This, in turn, may lead to large deformations, and thus poor shape quality or even mirror damage. Several works provide a comprehensive overview of the available different secondary reflector materials and different CSP configurations, which confirms the importance of analysing secondary concentrators, by simulating [4] and testing [1], [2], [9], [4] relevant operating conditions. Having a robust thermal-structural design workflow allows the design of mirrors to withstand a higher concentration ratio at the secondary reflector, i.e., the ratio between areas of primary and secondary mirrors, thus helping to improve plant competitiveness and decrease the levelized cost of heat (LCOH), as a consequence of the reduction in overall beam-down tower dimensions and shadowing losses. In this context, the authors investigated the optimisation of the structural design of a secondary mirror substrate consisting of an AISI 304 steel plate coated with a highly reflective mirror layer, with an expected reflectance greater than 90%. The aim of the investigations is to define the secondary mirror-optimized structural design, to withstand thermo-mechanical stresses, working with daily thermal cycles.

2. Methodology

This section is going to focus on the methodology employed for the development of this study. It consists of three subsections: the description (i) of the original design and (ii) of the developed structural model under optimisation, and (iii) the algorithm.

2.1. Original design

The original design of the secondary mirror consists of an AISI 304 plate with 5mm thickness with one side treated with Physical Vapour Deposition (PVD) to obtain a reflectance of about 90%, acting as a mirror. On the other side, there are brackets for mounting the secondary mirror on its support. The mirror is shown in Figure 1 while the mirror-support assembly is depicted in Figure 2. The secondary mirrors are placed at 12m height and oriented of 13.5° with respect to the horizontal, as shown in Figure 1. The mirrors are subjected to their own weight and to the environmental and operational conditions, that are the wind and the temperature. The temperature acts as a daily thermal cycle of 200°C, while the foreseen wind speeds are 45m/s for 3s gusts at 10m above the ground and 30m/s (10min temporal mean) at 10m above the ground, as reported in Table 1.

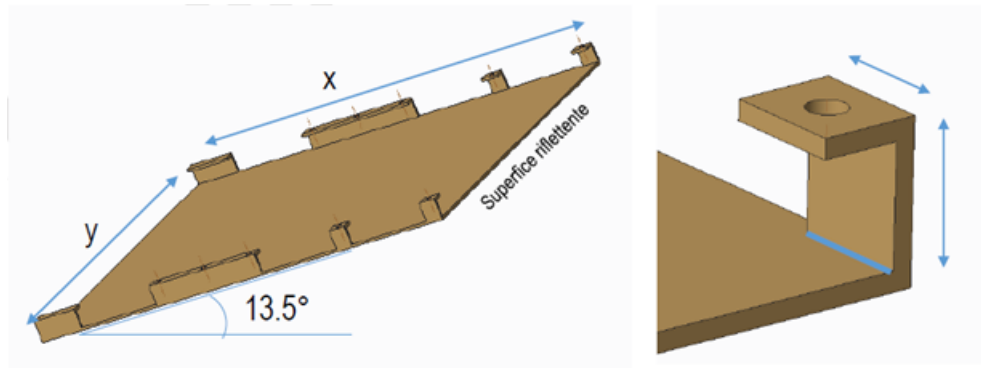


Figure 1: Original design of the secondary mirror.

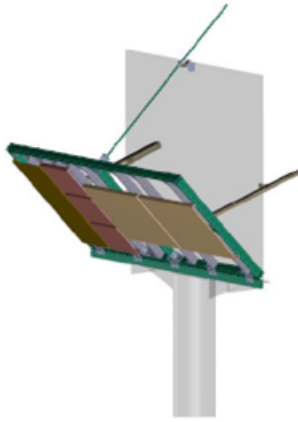


Figure 2: Assembly of the starting secondary mirror on the support.

Table 1: Foreseen wind speed.

Parameter	Value
Basic wind speed (3s gust) at 10m above ground (v_b)	45m/s
Basic wind speed (10min mean) at 10m above ground (v_b)	30m/s

2.2. Developed structural model

The structural model under optimisation is developed in Abaqus. The plate and the brackets have been modelled as 2D shell planar thanks to the intrinsic slenderness of these structures, allowing for computational advantages in terms of both costs and time. The plate dimensions have been fixed to $800 \times 800 \text{ mm}$, as reported in Figure 3, while the plate thickness is one of the parameters under optimisation. The latter is supposed to vary between 1 mm and 5 mm with increments of 1 mm . The brackets are C-shaped, as shown in Figure 4, and their semi-height H , which is highlighted in the aforementioned figure, varies from 40 mm to 100 mm with increments of 10 mm . The bracket thickness varies as the plate one, i.e., from 1 mm to 5 mm with steps of 1 mm . The width of the bracket is constant and equal to 50 mm , in the plane perpendicular to Figure 4. The number of brackets can vary, allowing one for choosing the best configuration available. Referring to Figure 5, the brackets number ($\#C$) can vary from 6 to 9 where if:

- $\#C = 6$, the highlighted brackets are excluded from the configuration.
- $\#C = 7$, the highlighted central bracket is included in the configuration.
- $\#C = 8$, only the highlighted central bracket is excluded from the configuration.
- $\#C = 9$, all the brackets are included in the configuration.

The brackets are connected to the plate using the tie kinematic contact by choosing the plate as the master element and four points of the bracket for the slave elements, as depicted in Figure 6, to represent the welding of the bracket on the plate. This contact type allows for the computation of the reaction forces at the welds and, thus, to perform the safety assessment at the weld.

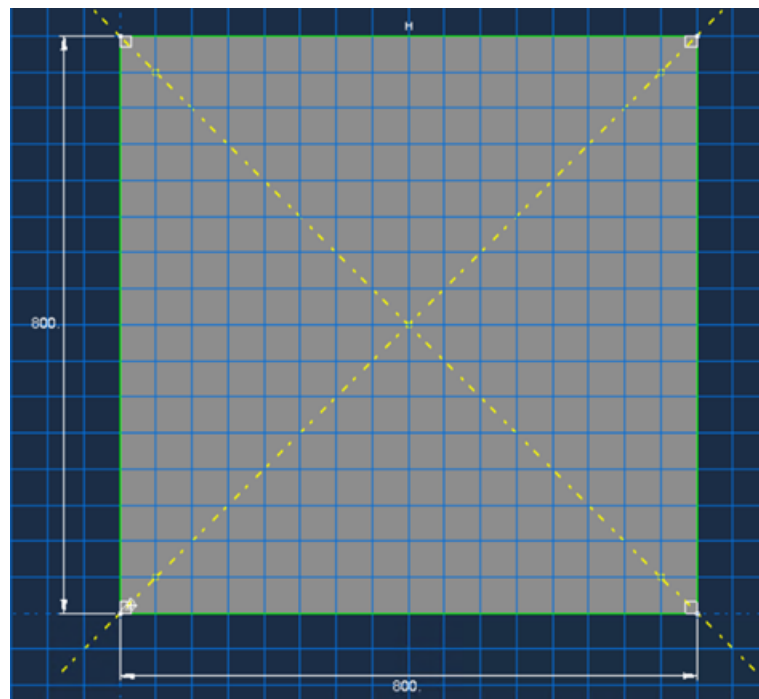


Figure 3: Assembly of the starting secondary mirror on the support.

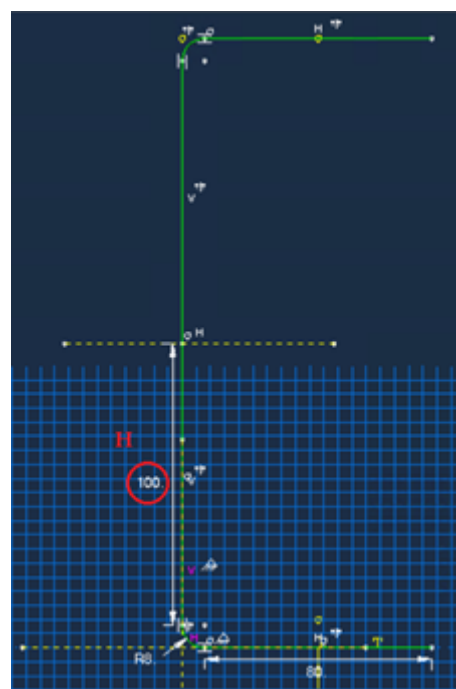


Figure 4: Assembly of the starting secondary mirror on the support.

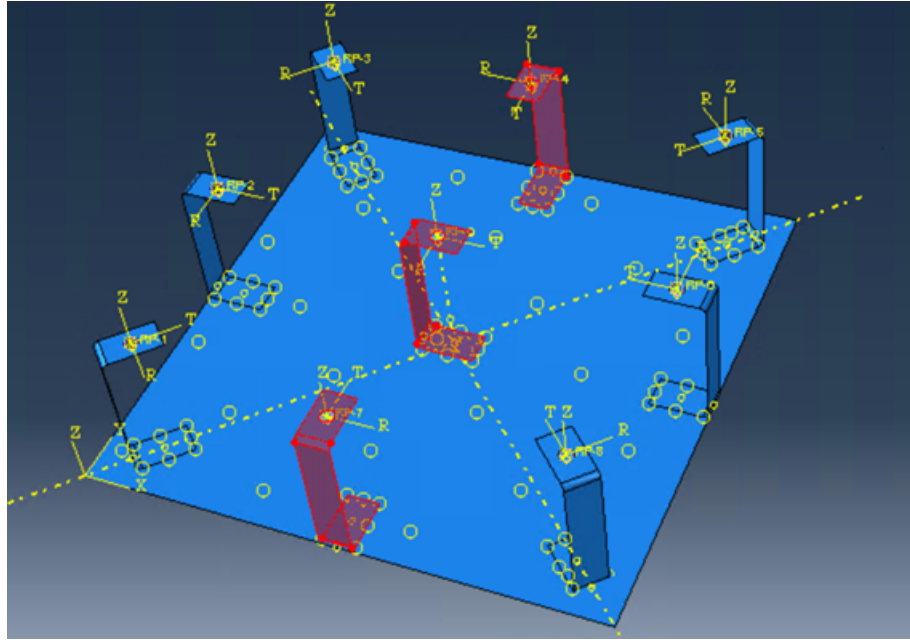


Figure 5: Assembly of the C-shaped brackets on the plate. The brackets highlighted in red are the ones which are included or excluded from the analysis depending on the configuration.

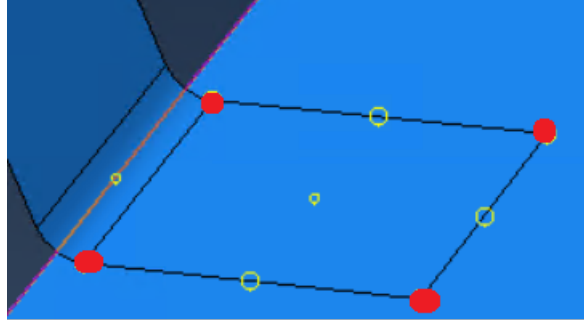


Figure 6: Tie contact modelling between plate and brackets.

Resuming, there are a total of 4 parameters under optimisation which are the plate thickness and the brackets' number, semi-height, and thickness, as reported in Table 2, for a total of 700 possible configurations. To evaluate the structural performances of each configuration loads are applied to the structure, in particular, other than the gravity, there are:

- the thermal load is applied by imposing a homogeneous temperature of 200°C to both plate and brackets.
- the wind is applied as the drag and lift pressures acting on the plate surface in two different wind conditions:
 - mean wind, with a speed of 13km/h .
 - maximum wind, with a speed of 100km/h .

The loads are applied singularly to observe the effects of each condition on the structure.

Table 2: Parameters under optimisation.

	#C	Bracket thickness [mm]	Bracket semi-height [mm]	Plate thickness [mm]
min	6	1	40	1
max	9	5	100	5
step	1	1	10	1

To perform automatically the analysis in each configuration, a Python code has been used which loads the Abaqus CAE model and varies the parameters, performing simulations. The number of brackets changes by

activating and deactivating the contact according to the configuration.

2.3. Algorithm

A Python algorithm has been developed to analyse the results in each configuration. The use of algorithms for data processing while respecting constraints represents a consolidated practice in the field of engineering. Specifically, within the scope of structural engineering, this class of algorithms is typically employed to guide the design of a structure towards the optimization of certain desired properties, such as minimizing its weight and/or maximizing its stiffness (thus minimizing the expected deformation when the structure is subjected to predetermined loads). In this context, integrating the design phase of the secondary mirror structure with optimization algorithms represents a valid alternative to achieve optimal design conditions. In this specific case, the optimisation process aims to identify the set of structural solutions that minimise the stress state and the deformation to which the analysed structure is subjected while respecting the required constraints. To this end, a Python framework is defined to optimise the secondary mirror.

2.3.1 Optimisation algorithm

In a generic optimization process, the following entities are identified:

- Design variables: These are the quantities whose values are modified in the optimisation process to determine the optimal solution to the problem. These variables can be discrete or vary within a continuous range of values.
- Objective function: The objective function is the function that the optimiser aims to minimise (or maximise). It depends on the values of the design variables. In the case where more than one objective function is considered within the optimization process, it is referred to as multi-objective optimization.
- Constraints: Constraints represent conditions that limit the search space for the optimal solution. They are expressed in the form of equations and/or inequalities, generally as a function of constant parameters, design variables, and/or the objective function.

In this work, the identified design variables are the bracket (i) number, (ii) semi-height, and (iii) thickness as well as the (iv) plate thickness, as reported in Table 2. The number of brackets can only take integer values, while for the other variables, it has been assumed that the same holds true in order to reduce the computational load caused by a large number of combinations and to obtain standard values for the implementation phase of the proposed design solution. The implemented algorithm consists of the following steps:

- The amplification of the stress state is carried out according to the coefficients defined in Eurocode 3 [10], specifically $c_{weight} = 1.4$ for the stresses caused by the weight force and $c_{wind} = 1.5$ for those due to wind action.
- Sum of the stress state obtained in the different loading conditions for all the components.
- Sum of plate displacements under the different loads.
- Evaluation of the slope deviation [11],[12], that is the angle between the actual and ideal surface normal.
- For each configuration, check that
 - maximum stress $\sigma_{max} \leq 85MPa$ for each component.
 - plate slope deviation $SDx_{rms} \leq 1mrad$.
- If all the checks are satisfied, then the configuration is approved by the algorithm.

The evaluation of the slope deviation is described in Equations 1, 2, and 3, where the term associated with the ideal condition in Equation 1 is equal to zero since, ideally, the plate is flat. The final slope deviation value is the larger one between SDx_{mean} and SDx_{rms} .

$$sdx = \left(\frac{d}{dx} z \right)_{measured} - \left(\frac{d}{dx} z \right)_{ideal} \quad (1)$$

$$SDx_{mean} = \frac{1}{A} \iint sdx^2 dx dy \quad (2)$$

$$SDx_{rms} = \frac{1}{\sqrt{A}} \sqrt{\iint sdx^2 dx dy} \quad (3)$$

3. Results

The results of the proposed framework are presented in this section. Figure 7 shows the configurations which satisfy the constraint on slope deviation, meaning that this constraint is very restrictive since only 45 out of 700

configurations pass this check. In Figure 8 it is possible to see the maximum stresses acting on the plate in the configurations that satisfy the constraint on the slope deviation by summing the contributions of the three loads. To analyse the influence of the design variables on the slope deviation, a Pareto analysis has been carried on on the configurations that satisfy the constraint on this quantity. The results are shown from Figure 9 to Figure 12, and it is possible to notice that the configurations with 9 brackets are the most approved, together with the ones with the thickest plate and highest brackets, while thin brackets with a thickness of 2mm seem to be suggested. However, when considering also the stress state on the brackets the situation changes and, analysing the stress constraint on these components, the configurations approved pass from 45 to 4, which are reported in Table 3. Also for the final configurations the analysis of the influence of each design variable on the optimisation output is conducted, and the results are shown from Figure 13 to Figure 16. The values of slope deviation for the final configurations are shown in Figure 17. The results of the simulations are presented just for one configuration, the *C_9_TC_4_HC_100_TP_4*, i.e. the last configuration of Table 3, as an example and separately for the three loading conditions and for each of the three analyzed quantities: Von Mises stresses [MPa] from Figure 18 to Figure 20, displacements [mm] from Figure 21 to Figure 23, and rotations [rad] from Figure 21 to Figure 23. From the results, it can be noted that the "C" brackets are the most stressed components, especially around the hole for bolting to the support. This point does not pose particular problems since the bolting has not been modelled, and the tightening of the brackets to the support prevents the intensification of stresses that occurs during the simulation, thanks to the compressive preload necessary for tightening. All results are shown on the deformed plate.

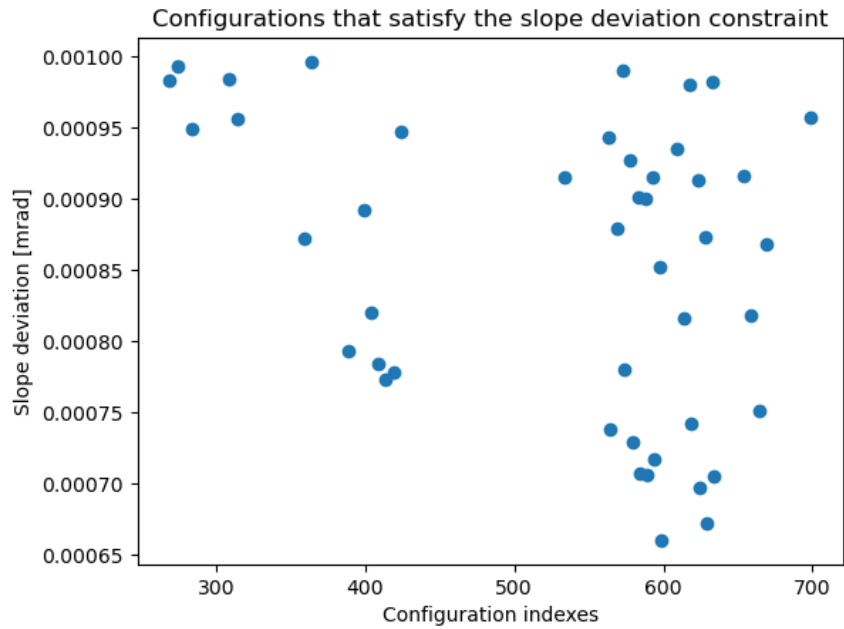


Figure 7: Influence of slope deviation constraint.

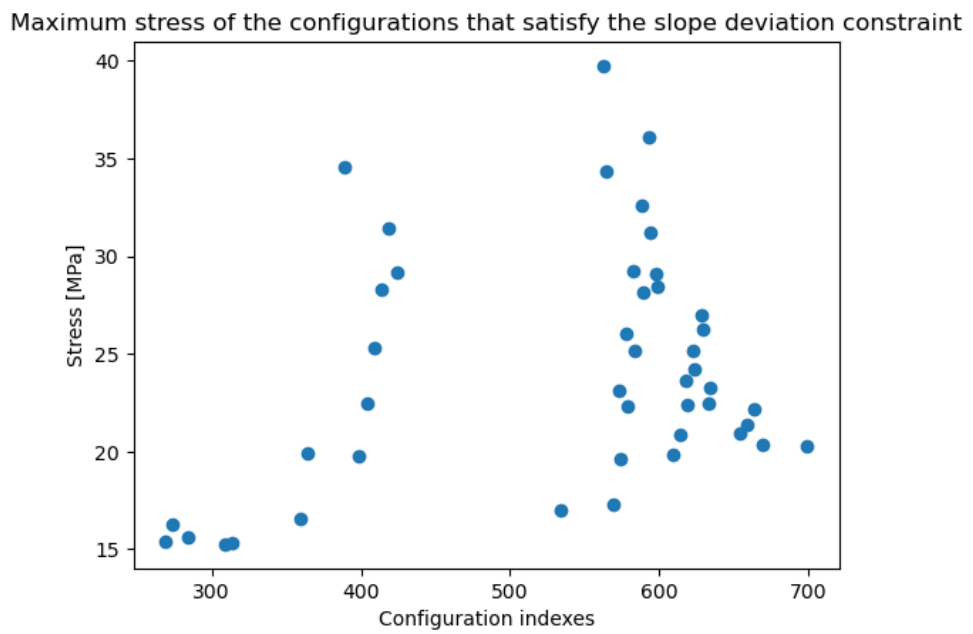


Figure 8: Comparison between the plate maximum stresses in the configurations that satisfy the constraint on the slope deviation by summing the contributions of the three loads.

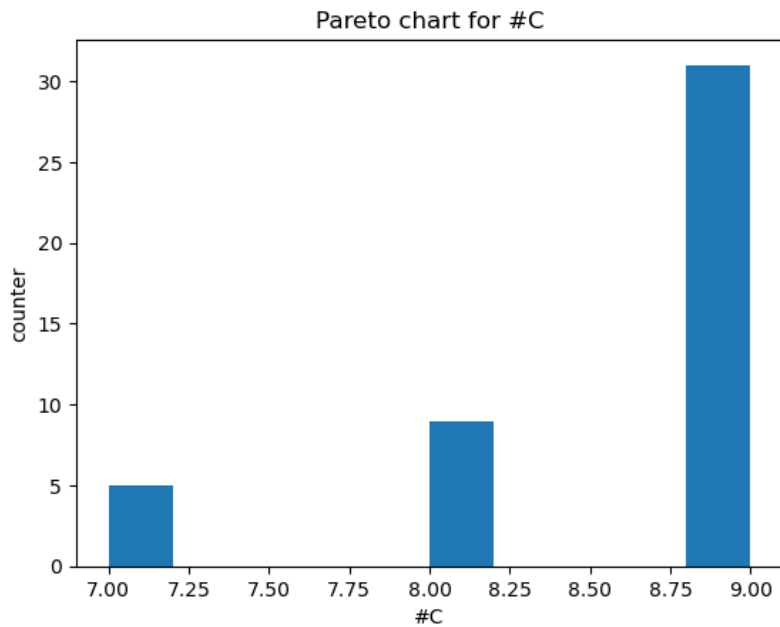


Figure 9: Influence of the bracket number on the slope deviation constraint.

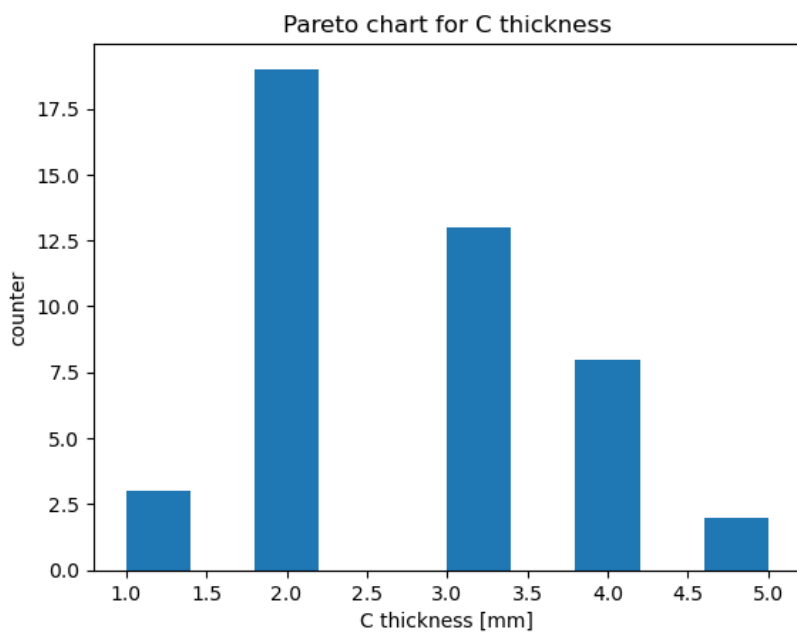


Figure 10: Influence of the bracket thickness on the slope deviation constraint.

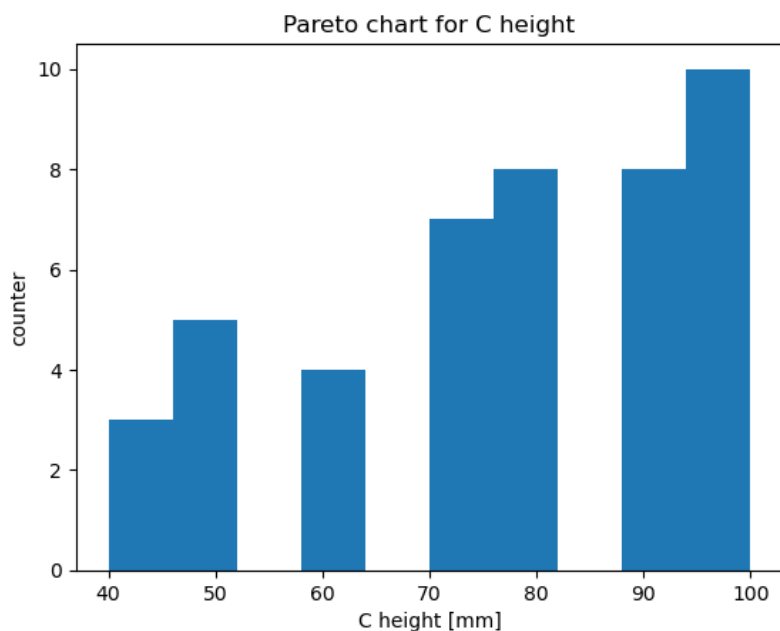


Figure 11: Influence of the bracket height on the slope deviation constraint.

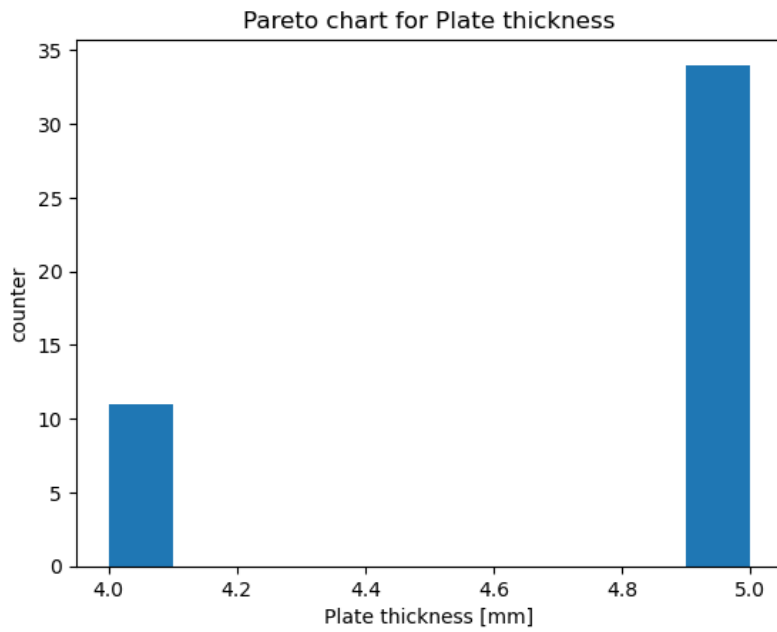


Figure 12: Influence of the plate thickness on the slope deviation constraint.

Table 3: Configurations selected by the optimisation algorithm.

$\#C$	Bracket thickness [mm]	Bracket semi-height [mm]	Plate thickness [mm]
8	3	100	5
9	3	100	4
9	3	100	5
9	4	100	4

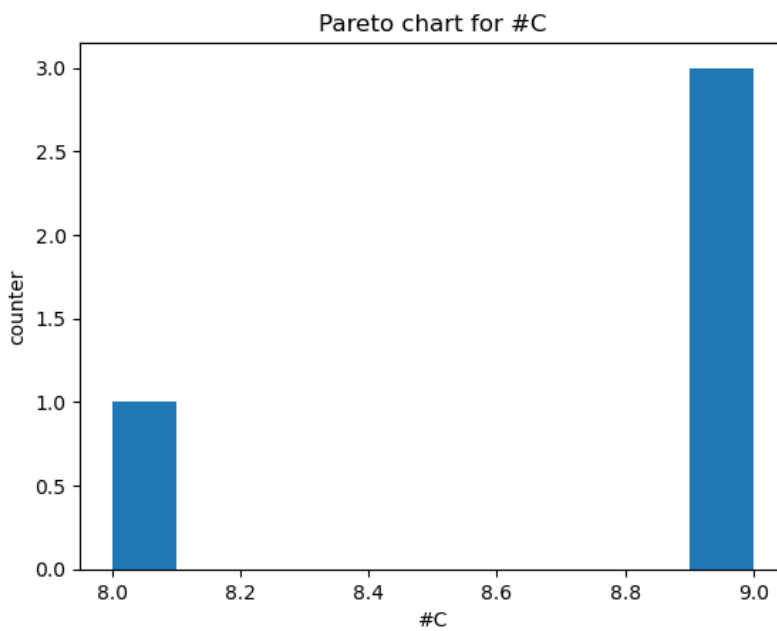


Figure 13: Influence of the bracket number on the approved configurations.

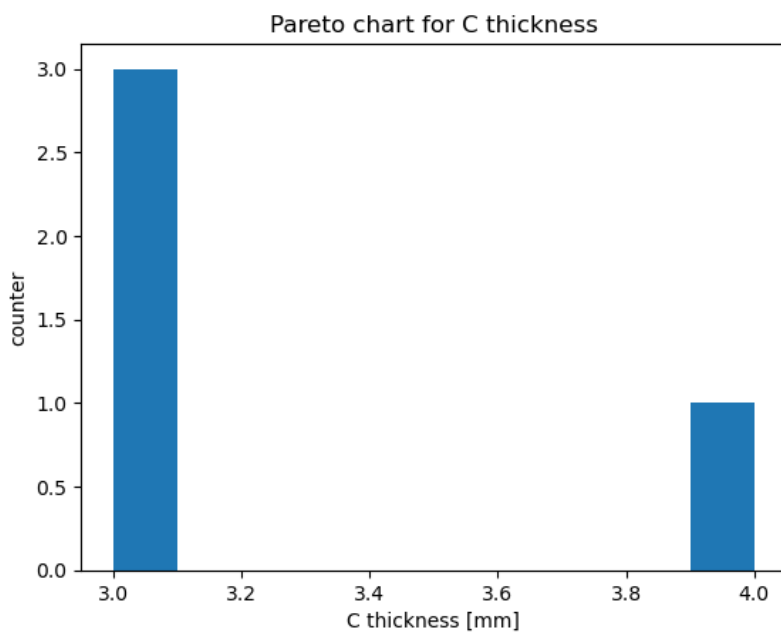


Figure 14: Influence of the bracket thickness on the approved configurations.

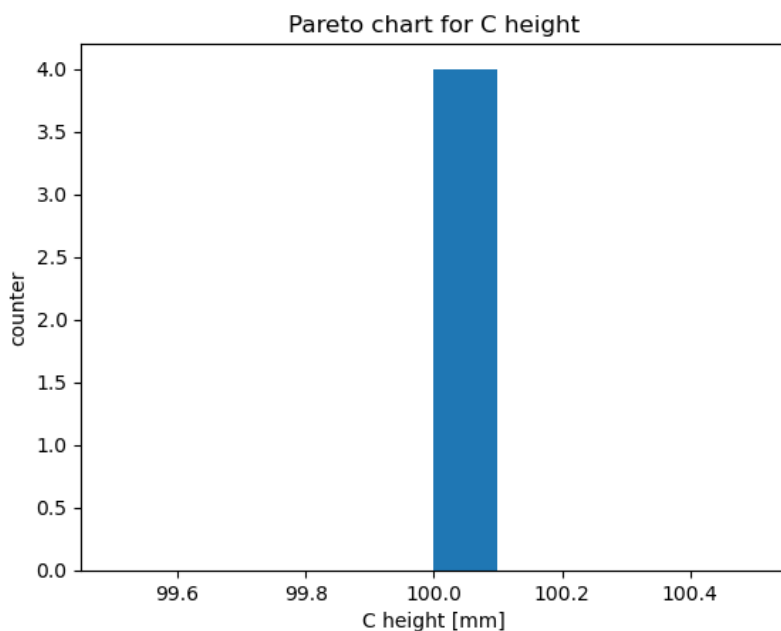


Figure 15: Influence of the bracket height on the approved configurations.

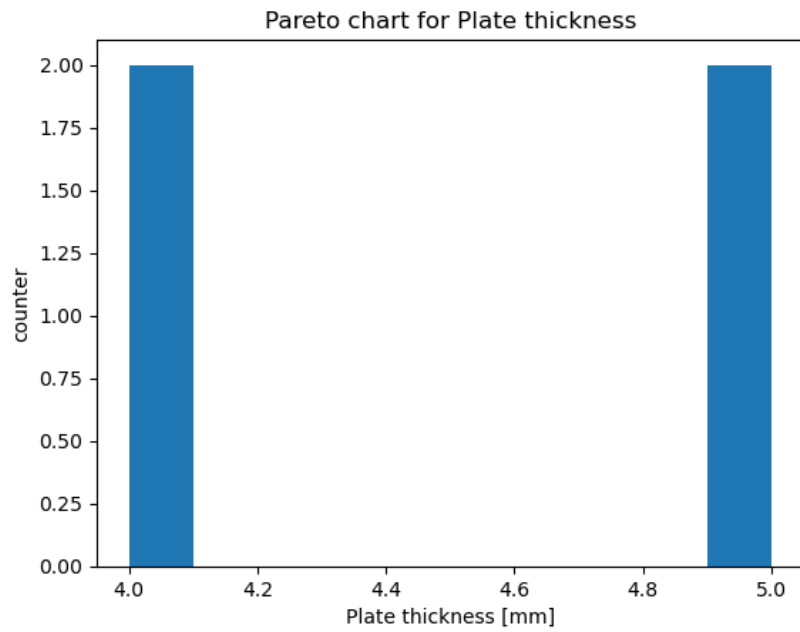


Figure 16: Influence of the plate thickness on the approved configurations.

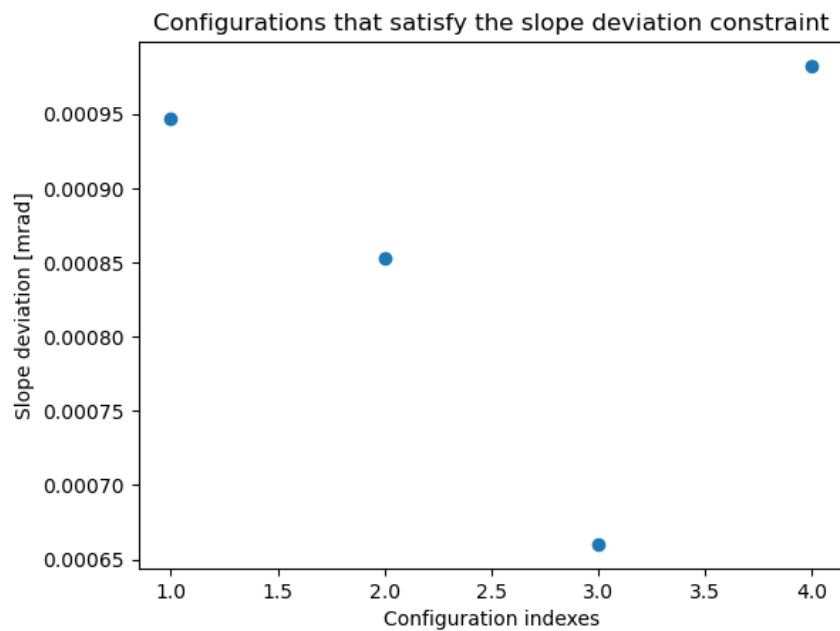


Figure 17: Comparison between the slope deviation in the selected configuration, reported in the same order as Table 3, by summing the contributions of gravity, thermal load, and wind.

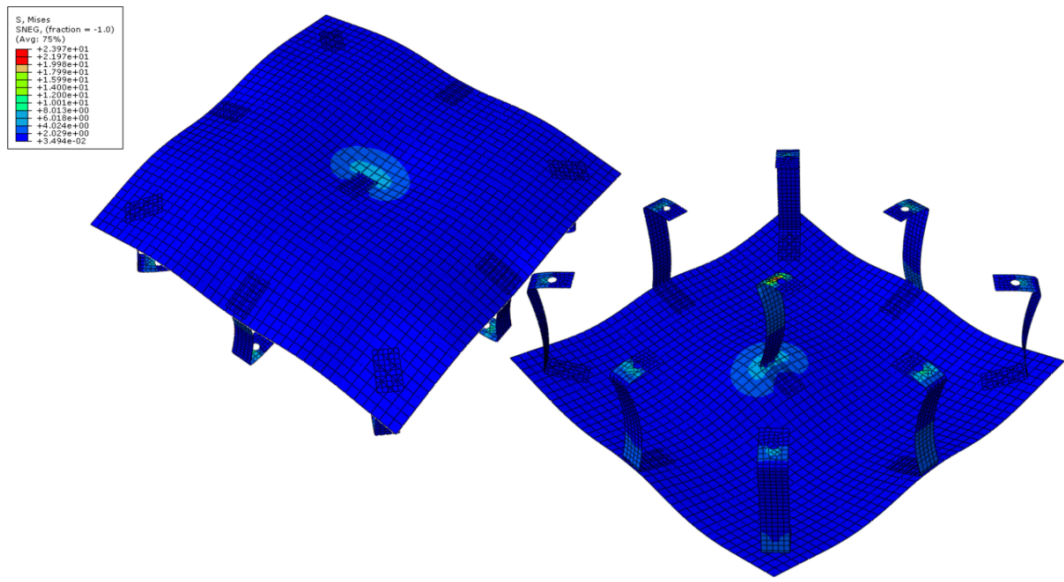


Figure 18: Von Mises stresses [MPa] for the secondary mirror when subjected to its own weight.

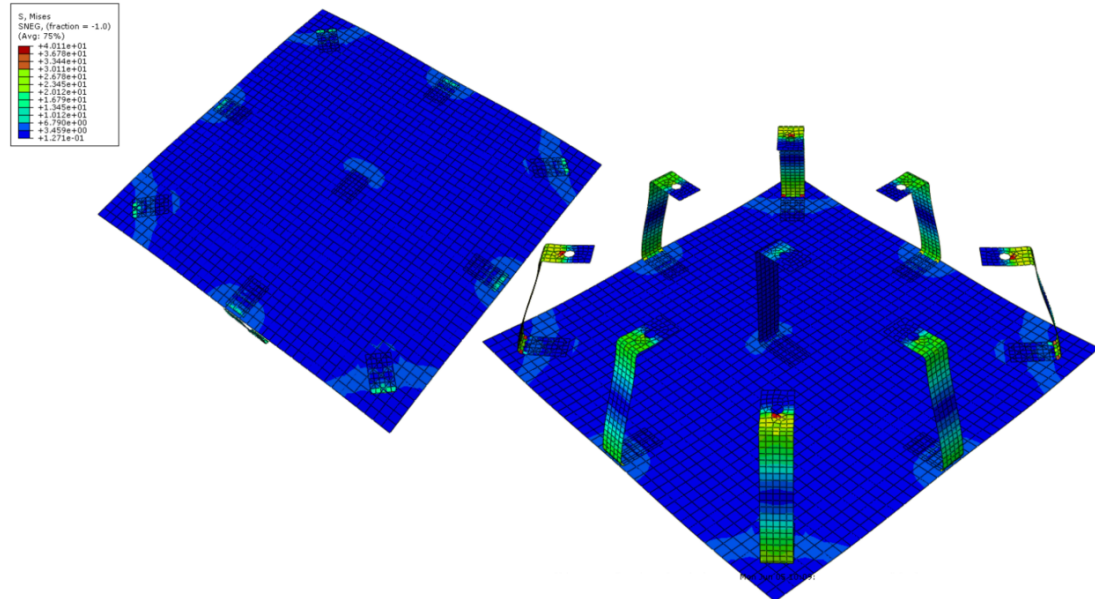


Figure 19: Von Mises stresses [MPa] for the secondary mirror when subjected to the thermal load.

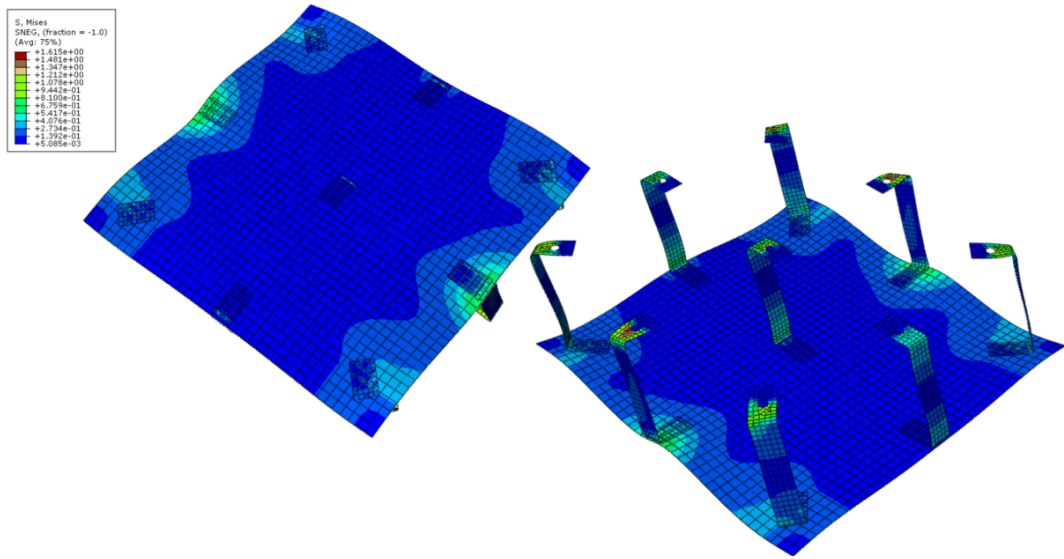


Figure 20: Von Mises stresses [MPa] for the secondary mirror when subjected to the operative wind ($13km/h$).

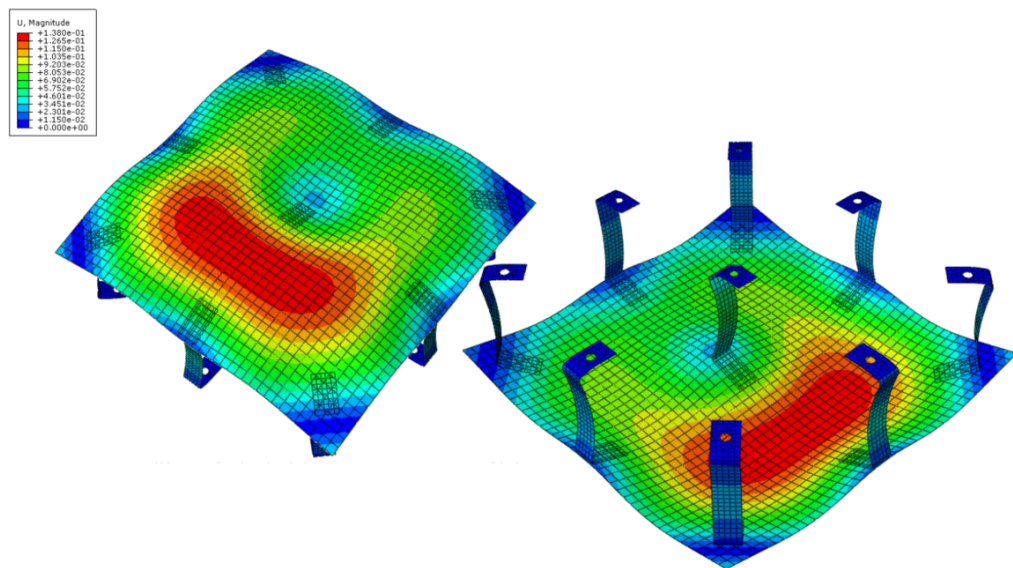


Figure 21: Displacement [mm] for the secondary mirror when subjected to its own weight.

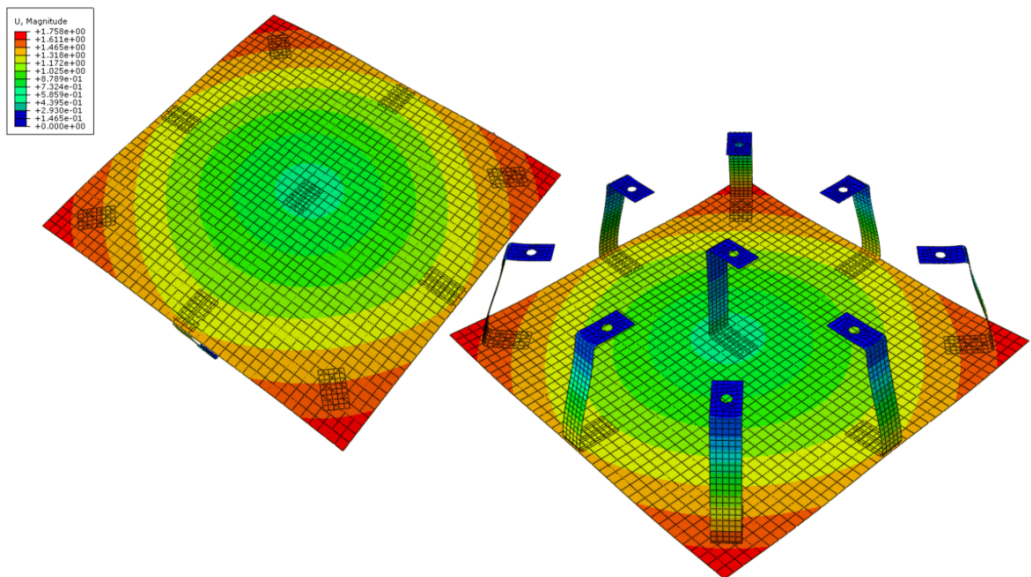


Figure 22: Displacement [mm] for the secondary mirror when subjected to the thermal load.

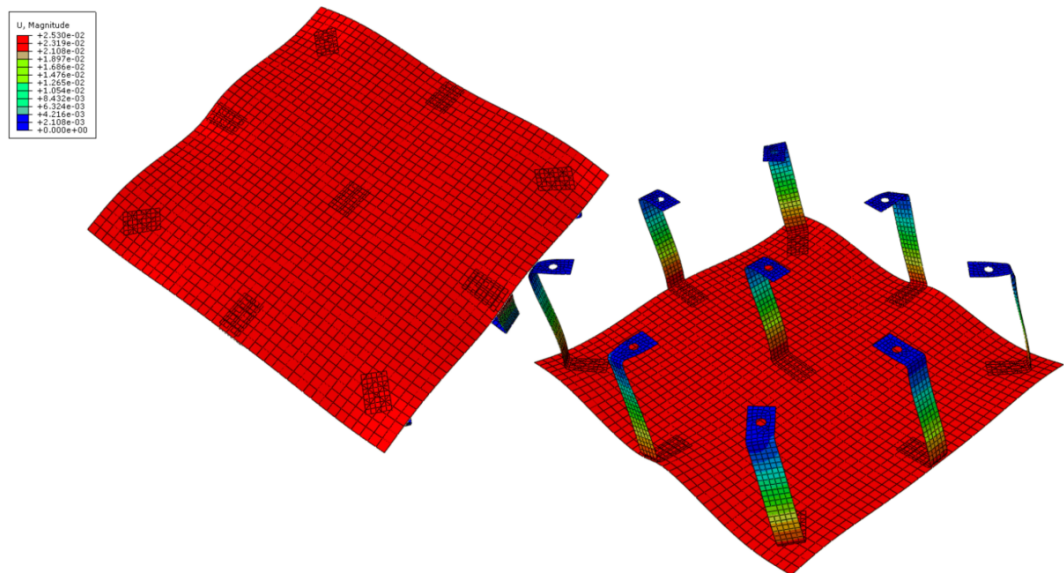


Figure 23: Displacement [mm] for the secondary mirror when subjected to the operative wind (13km/h).

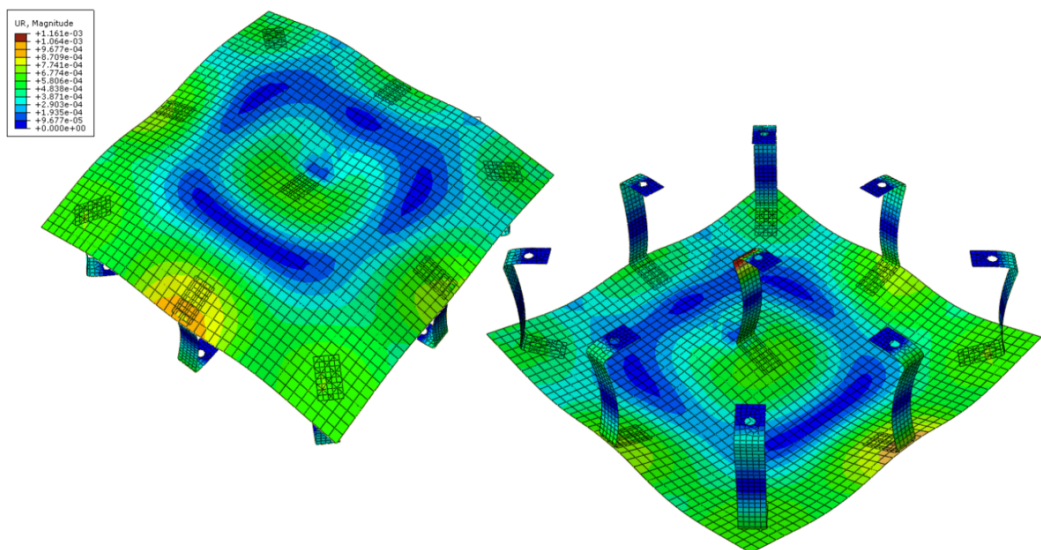


Figure 24: Rotation [rad] for the secondary mirror when subjected to its own weight.

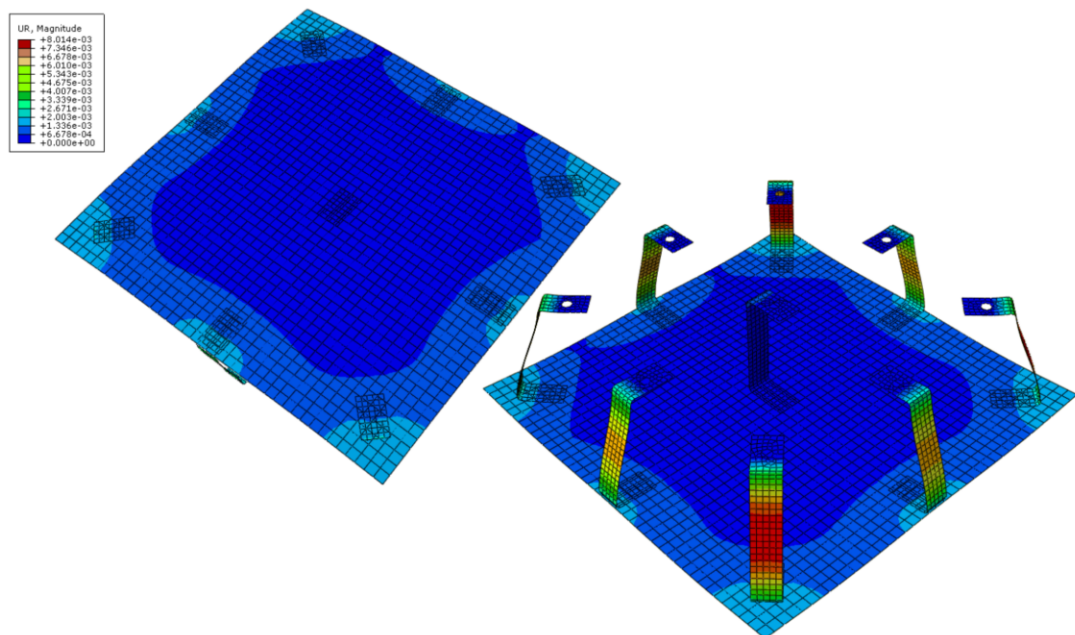


Figure 25: Rotation [rad] for the secondary mirror when subjected to the thermal load.

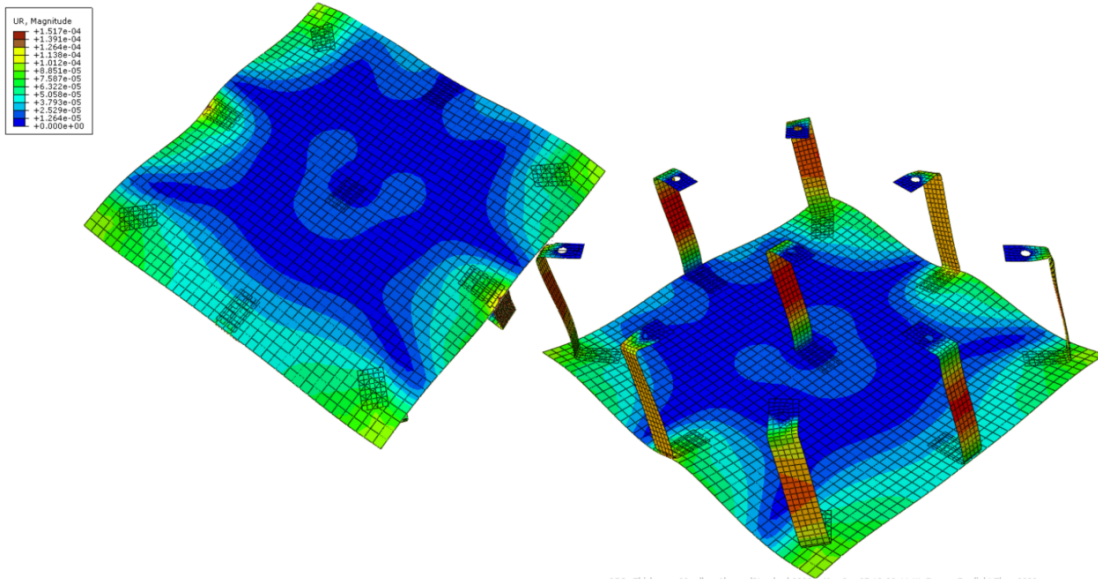


Figure 26: Rotation [rad] for the secondary mirror when subjected to the operative wind ($13\text{km}/\text{h}$).

4. Discussion

This study describes the framework developed to conduct the optimization of the secondary mirror, which consists of the mirror itself and the brackets that allow it to be fixed to the supports. The structural model, implemented in Abaqus, allows the evaluation of several indicators of structural performance related to the adopted configuration, such as deformation (rotation), displacements, and stress state generated by the applied loads. The results showed that the optimal configurations are the ones with the highest number of brackets, 8 and 9, medium thick brackets, i.e., 3mm and 4mm , and with the highest plate thicknesses, from 4mm to 5mm , but there is not a clear optimum between these configurations. On the contrary, the optimal value for the bracket semi-height has been found and is 100mm . Further investigations can be done by decreasing the increment for the thicknesses and for the semi-height, as well as extending the bracket semi-height range. The choice of the final design can not be performed without considering also the optical efficiency in the deformed condition of the secondary mirror, even if this is preliminarily performed by imposing a constraint on the slope deviation in the optimisation algorithm. The tools implemented in the environment described in this study have strong development potential. For example, the optimisation algorithm is flexible and capable of handling a process based on the satisfaction of an unlimited number of constraints. In this perspective, new constraints could be added, or the algorithm could be adapted to new case studies. For instance, a similar methodology could be developed to maximize the optical efficiency of individual mirrors. Furthermore, it is possible to consider integrating the structural model implemented in Abaqus by adding design variables, moving towards a more comprehensive but computationally expensive optimization process.

References

- [1] S. Gledhill, C. Hildebrandt, R. Uhlig, J. Wette and F. Sutter; “Secondary reflector tested at high temperatures and high radiation intensities”, SolarPaces, 2021.
- [2] A. Fernandez-Garcia, M. Cantos-Soto, M. Roger, C. Wieckert, C. Hutter and L. Martinez-Arcos; “Durability of solar reflector materials for secondary concentrators used in CSP systems”, Solar Energy Materials and Solar Cells, 2014.
- [3] G. A. C. - I. o. S. Research, «Solar thermal power plants» 2021
- [4] Rami Ben-Zvi, Akiba Segal, Michael Epstein, “Beam-Down Mirror: Thermal and Stress Analyses”, J. Sol. Energy Eng. Volume 131, Issue 4 November 2009.
- [5] A. Zanut, M. Binotti and A. Giostri; “Design and optimization of a point focus Beam-Down system”; Thesis, PoliMi, 2021.

- [6] N. Calvet, A. H. Slocum, A. Gil, B. Grange, R. Lahlou, T. T. Hamer, M. Diago, M. Tetreault-Friend, D. S. Codd, D. L. Trumper, and P. R. Armstrong; “Dispatchable Solar Power Using Molten Salt Directly Irradiated from Above,” *Solar Energy*, Volume 220, 15 May 2021, Pages 217-229.
- [7] M. Diago, N. Calvet, P. R. Armstrong; “Net Power Maximization in a Faceted Beam-down Solar Concentrator,” *Solar Energy*, Volume 204, 1 July 2020, Pages 476-488.
- [8] R. Chirone, P. Salatino, P. Ammendola, R. Solimene, M, Magaldi, R. Sorrenti, G. Di Michele, F. Donatini, *Engineering Conferences International*, 2013.
- [9] R. Lahlou, P. Armstrong, N. Calvet, A. Slocum and T. Shamim; “Testing of a secondary concentrator integrated with a beam-down tower system under non-liquid cooling strategies”, *SolarPaces*, 2017.
- [10] EN 1993-1-1:2005 +A1:2014. Eurocode 3: Design of steel structures [Online]. Available: <https://eurocodes.jrc.ec.europa.eu/EN-Eurocodes/eurocode-3-design-steel-structures>.
- [11] M. Röger, “Heliostat Performance Testing Guideline - Status Update in SolarPaces Task III Workshop”, Santiago de Chile, September 25, 2017. <http://elib.dlr.de/115415/>.
- [12] Solar Paces Task III Measurement Of Solar Weighted Reflectance Of Mirror Materials For Concentrating Solar Powertechnology With Commercially Available Instrumentation: http://www.solarpaces.org/Tasks/Task3/Interim_Reflectance_Guideline.pdf.